

INTER-AMERICAN TROPICAL TUNA COMMISSION

SCIENTIFIC ADVISORY COMMITTEE

NINTH MEETING

La Jolla, California (USA)

14-18 May 2018

DOCUMENT SAC-09-09

SPATIOTEMPORAL DYNAMICS OF THE DOLPHIN-ASSOCIATED PURSE-SEINE FISHERY FOR YELLOWFIN TUNA IN THE EASTERN PACIFIC OCEAN

Haikun Xu, Cleridy E. Lennert-Cody, Mark N. Maunder, and Carolina Minte-Vera

CONTENTS

Summary 1

1. Background 1

2. Data and methods 2

3. Results..... 4

4. Discussion 4

Acknowledgements..... 6

References 6

Figures..... 7

SUMMARY

Including spatiotemporal dynamics in the standardization of catch-per-unit-effort (CPUE) data to produce an index of relative abundance is important to ensure that the index more completely represents the abundance of the whole population rather than just the component of the population targeted by the fishery (Maunder *et al.* 2017). This is particularly important when there are substantial spatial variations in the size structure of a stock and the areas in which it is caught, as is the case for yellowfin tuna (*Thunnus albacares*) in the eastern Pacific Ocean (EPO). The stock assessment needs to appropriately differentiate between the size composition represented by the index and the size composition represented by the catch, and this can only be done by applying spatiotemporal models (Maunder *et al.* 2017). To standardize the index of relative abundance for yellowfin, we applied a spatiotemporal delta-generalized linear mixed model to the catch and effort data of the dolphin-associated fishery for yellowfin in the EPO during 1975-2016. In comparison to the nominal CPUE used in the stock assessment, the standardized CPUE suggested higher initial abundances and lower terminal abundances. Also, the confidence interval of the standardized CPUE varied over time, being markedly larger in the first decade than in the last decade of the study period. When applied to the length-composition data for yellowfin in the EPO north of the Equator, the spatiotemporal model suggested that yellowfin in that region was spatially segregated by length.

1. BACKGROUND

Indices of relative abundance directly inform trends in population biomass and are a key input in integrated fisheries stock assessments (Francis 2011). Fishery-independent data are not available for the assessment of yellowfin tuna in the EPO, so indices of relative abundance are derived solely from

fishery-dependent CPUE data. CPUE data need to be standardized to eliminate factors other than abundance that could influence the index, and accounting for spatial effects is important in the standardization of CPUE. Because the spatial coverage of CPUE data is relatively sparse for all the fisheries that catch yellowfin in the EPO, the standardization of fishery-dependent CPUE data is particularly difficult for yellowfin. Length-composition data, which inform selectivity and year-class strength, are another important component of stock assessments, and spatiotemporal modeling of these data may lead to improved estimates of the overall size composition of the catch and the selectivity function for the index of abundance.

The dolphin-associated purse-seine fishery takes most of the catches of yellowfin in the EPO (IATTC 2017). In addition, two of the five indices of relative abundance used in the stock assessment are nominal CPUEs of the dolphin-associated purse-seine fisheries that operate in different regions of the EPO (Minte-Vera *et al.* 2017). In this study, we evaluate the spatiotemporal dynamics of yellowfin in the EPO based on the CPUE and length-composition data from vessels fishing primarily on dolphin-associated yellowfin. This fishery relies on the strong tuna-dolphin association in the tropical EPO (Scott *et al.* 2012), where the habitat of yellowfin is restricted to the warm and shallow mixed layer by the oxygen-poor waters underneath. Because of the large percentage of zero-value observations in the CPUE and length-composition data, we apply a spatiotemporal delta-generalized linear mixed model (using the R package VAST (Thorson *et al.* 2015)), to develop a standardized index of relative abundance and to estimate the length composition of yellowfin in the EPO. We chose VAST because of its ability to impute catch rates in unsampled regions based on the estimated spatial autocorrelation structure.

2. DATA AND METHODS

2.1. Index of relative abundance

The per-vessel catch (in metric tons) and effort (in days fishing) data that were used to estimate a standardized index of relative abundance for yellowfin in the EPO during 1975-2016 had a spatial resolution of $1^\circ \times 1^\circ$ and temporal resolution of 1 day. To control for differences in fishing strategies among vessels, we limited the data used in this analysis to vessels that made more than 75% of their sets on tunas associated with dolphins. The nominal CPUE for each vessel-day- 1° grid cell was computed as the ratio of the sum of the catch in all three set types (dolphin, floating-object, and unassociated) to effort. The fishing ground for yellowfin varied notably among quarters over the study period (Figure 1), so the CPUE data were modeled separately for each quarter. However, the current assessment of yellowfin uses the “quarter as year” approach, and thus the four indices of relative abundance, which have an annual time step, need to be combined into one overall index with a quarterly time step. We standardized the four indices of relative abundance over the same spatial domain, which includes all grid cells with at least one observation of yellowfin catch during 1975-2016 (Figure 2).

For the spatiotemporal model, the probability of positive catch (encounter probability) and the catch rate for positive catches were modeled separately in VAST, and it was assumed that the expected catch rate can be estimated as the product of the two components (Thorson *et al.* 2015). We specified the model for the encounter probability for sample i as

$$p_i = \text{logit}^{-1}(\beta_1(t_i) + L_{\omega_1}\omega_1(s_i) + L_{\varepsilon_1}\varepsilon_1(s_i, t_i) + L_{\delta_1}\delta_1(v_i))$$

where $\beta_1(t_i)$ is the intercept in year t_i , $\omega_1(s_i)$ is the spatial variation at location s_i , $\varepsilon_1(s_i, t_i)$ is the spatiotemporal variation at location s_i in year t_i , and $\delta_1(v_i)$ is the effect of vessel v_i on encounter probability. L_{ω_1} , L_{ε_1} , and L_{δ_1} are the coefficients used to standardize the variance of ω_1 , ε_1 , and δ_1 to be 1. The spatial and spatiotemporal residuals (random effects) for the encounter probability were assumed to be autocorrelated in space and to follow a multivariate normal distribution:

$$\begin{aligned}\omega_1 &\sim \text{MVN}(\mathbf{0}, \mathbf{R}_1) \\ \varepsilon_1(t) &\sim \text{MVN}(\mathbf{0}, \mathbf{R}_1) \\ R_1(s, s') &= \frac{1}{2^{m-1}\Gamma(m)} \times (\kappa_1 |\mathbf{H}(s - s')|)^m \times K_m(\kappa_1 |\mathbf{H}(s - s')|)\end{aligned}$$

where \mathbf{R}_1 and κ_1 are the correlation matrix and decorrelation distance, respectively, for both the spatial and spatiotemporal residuals, m represents Matern smoothness (fixed at 1), and K_m is the modified Bessel function of second kind. \mathbf{H} specifies geometric anisotropy, so $|\mathbf{H}(s - s')|$ is the distance between locations s and s' after considering geometric anisotropy. Similarly, we specified the model for the positive catch rate for sample i as

$$\begin{aligned}\lambda_i &= \exp(\beta_2(t_i) + L_{\omega_2}\omega_2(s_i) + L_{\varepsilon_2}\varepsilon_2(s_i, t_i) + L_{\delta_2}\delta_2(v_i)) \\ \omega_2 &\sim \text{MVN}(\mathbf{0}, \mathbf{R}_2) \\ \varepsilon_2(t) &\sim \text{MVN}(\mathbf{0}, \mathbf{R}_2) \\ R_2(s, s') &= \frac{1}{2^{m-1}\Gamma(m)} \times (\kappa_2 |\mathbf{H}(s - s')|)^m \times K_m(\kappa_2 |\mathbf{H}(s - s')|)\end{aligned}$$

where all the parameters have the same definitions as those in the encounter probability model.

The probability function of catch for sample i , c_i , is

$$\Pr(c_i = C) = \begin{cases} 1 - p_i & \text{if } C = 0 \\ p_i \times \text{lognormal}(c_i | \lambda_i, \sigma_i^2) & \text{if } C > 0 \end{cases}$$

For computational purposes, we used the k -means algorithm to cluster all sampling locations into a pre-specified number ($n_k = 400$) of spatial knots (k) (Figure 2), and assumed that both the spatial and spatiotemporal residuals were constant within each spatial knot. Under the k -means algorithm, the area (a) associated with each spatial knot is negatively correlated with the number of local observations. The total abundance for the entire spatial domain was then predicted to be

$$I(t) = \sum_{k=1}^{n_k} (a(k) \times d(k, t))$$

where $d(k, t) = p(k, t) \times \lambda(k, t)$ is the predicted catch rate in knot k and year t .

2.2. Length composition

The length-composition data for yellowfin in the EPO include the catch (in number) at length (in 1-cm intervals) and effort (in days fishing) data, by purse-seine set type, during 2000-2016, with a spatial resolution of $5^\circ \times 5^\circ$ and a quarterly temporal resolution. Estimates of the length composition for each quarter-year- 5° grid cell were obtained as follows. First, the length data, which were already raised to the total catch of the sampled wells, were summed over months of the same quarter within a set type-year- 5° grid cell. Because of differences in yellowfin length composition by set type (IATTC 2017), the length-composition data were then raised to the total catch of each set type in the quarter-year- 5° grid cell before summing across set types. The nominal catch rate for each grid cell and quarter was calculated as the ratio of total catch to total effort. As was done for the analysis of relative abundance, we limited the data used in this analysis to vessels that made more than 75% of their sets on tunas associated with dolphins. We also limited the data to those sets observed north of the Equator in quarter 2 (Figure 3, top). Finally, based on the cumulative distribution function of catch at length, we divided the catch data into nine length groups, with groups 1 and 9 representing the smallest and largest fish, respectively (Figure 4).

We specified the encounter probability and the positive catch rate for sample i as

$$p_i = \text{logit}^{-1} \left(\beta_1(l_i, t_i) + L_{\omega_1}(l_i)\omega_1(s_i, l_i) + L_{\varepsilon_1}(l_i)\varepsilon_1(s_i, l_i, t_i) \right)$$

$$\lambda_i = \exp \left(\beta_2(l_i, t_i) + L_{\omega_2}(l_i)\omega_2(s_i, l_i) + L_{\varepsilon_2}(l_i)\varepsilon_2(s_i, l_i, t_i) \right)$$

where l_i denotes the length group for sample i . All other parameters have the same definitions as those in the index of relative abundance model. We used the k -means algorithm to cluster all sampling locations into 30 spatial knots (Figure 3, bottom), and assumed that both the spatial and spatiotemporal residuals were constant within each spatial knot. The predicted catch rate for length group l in knot k and year t is given by

$$d(k, l, t) = p(k, l, t) \times \lambda(k, l, t).$$

To facilitate the comparison of historical mean predicted catch rates among the nine length groups, the predicted catch rate for each length group was then normalized by removing the mean and dividing by the standard deviation:

$$\log \left(d^*(k, l, t) \right) = \frac{\left(\log(d(k, l, t)) - \text{mean}(\log(d(\cdot, l, \cdot))) \right)}{\text{sd}(\log(d(\cdot, l, \cdot)))}$$

3. RESULTS

The spatial distribution of predicted catch rates during 1975-2016 showed large year-to-year variations in all four quarters (Figures 5a-d). The historical mean predicted catch rate was higher north of the Equator, especially during quarters 2 and 3 (Figure 6, left column). Moreover, the highest predicted catch rates north of the Equator were consistently located around 10°N, where sea surface temperatures (SSTs) were high (Figure 6, right column) and the depth of the thermocline (TCD) was shallow (Figure 6, middle column). In fact, the regions of highest mean predicted catch rates all had a strong zonal component, regardless of quarter, probably because environmental conditions (*e.g.* SST and TCD) were more consistent east-to-west than north-to-south.

Based on the predicted catch rate for each quarter, we computed the standardized index of relative abundance for 1975-2016 with a quarterly time step (Figure 7). While the year-to-year variation in the standardized and nominal CPUE were generally in accordance with each other, the nominal CPUE tended to be lower and higher, respectively, than the standardized CPUE before 1985 and after 2005 (Figure 7). In other words, the nominal CPUE under-estimated initial abundances and over-estimated terminal abundances in comparison to the standardized CPUE. The noticeable difference between the two CPUEs underlines the importance of standardizing CPUE.

Spatial segregation of yellowfin by length was found in the predicted spatial distribution of historical mean catch rate at length (Figure 8). Specifically, the rate for small yellowfin (<95 cm) was predicted to be high in the coastal region off Mexico, but low in the pelagic region west of 120°W and the equatorial region south of 5°N, whereas for the largest yellowfin (>115 cm) it was predicted to be high in the latter two regions and low in the former. There was no strong spatial pattern for medium-sized yellowfin (95-115 cm).

4. DISCUSSION

4.1. Potential biases in the standardized CPUE

In our standardization procedure, we fitted each quarter's yellowfin fisheries data to the spatiotemporal model separately, and then combined the four annual indices of relative abundance into one quarterly

index for the current stock assessment model, which has a quarterly time step. This procedure includes three assumptions that could bias the results. First, catchability was assumed to be the same for the four quarters, but it could be quarter-specific: the fishing ground of the dolphin-associated yellowfin fishery and the environmental conditions that may affect the catch rate of the fishery both had a pronounced seasonal cycle. Second, the imputed catch rates for the unsampled region beyond the spatial extent of the data could be biased in different ways by quarter, since the region without fisheries data is quarter-specific. To ensure that the spatial domain over which the index of relative abundance was standardized is the same for all four quarters, it was specified by aggregating all fishing locations in the EPO during 1975-2016. However, the spatial distribution of fishing activity varied among quarters, so it was necessary to impute the quarterly catch rate for the unsampled region from sample data at neighboring locations and the estimated spatial autocorrelation structure. In the model, the spatial autocorrelation structures for both the encounter probability and the positive catch rate were assumed to be constant across space (*i.e.*, independent of spatial location). Any violation of this assumption could lead to biased imputation of catch rates and, consequently, a biased index of relative abundance for each quarter. If the biases in the indices of relative abundance were inconsistent among the four quarters, the combined relative index to be used in the stock assessment would be biased as well. Third, VAST assumed that the autocorrelation patterns in the spatial and spatiotemporal residuals were the same, which was not necessarily the case for yellowfin in the EPO. Since the spatial and spatiotemporal residuals for yellowfin were likely to be affected by different environmental processes (static vs. dynamic), their autocorrelations in space could also be different.

4.2. Standardized CPUE vs. nominal CPUE

Despite the potential biases noted above, the CPUE standardized by this spatiotemporal approach represents an improvement over the nominal CPUE used in the current stock assessment, from at least three perspectives. First, the spatiotemporal approach can account for vessel effects on catchability. Lennert-Cody *et al.* (2013) showed that ignoring these effects on the catchability of the dolphin-associated yellowfin fishery led to overly-optimistic estimates of CPUE for the most recent years. Second, it can account for preferential sampling, which is a common phenomenon in fishery-dependent catch and effort data. The nominal CPUE is based on the data from regions with fishing activity, where the abundance of yellowfin is likely to be higher than in the rest of the EPO. In contrast, the spatiotemporal approach imputes catch rates in regions without fishing activity, and calculates the standardized CPUE based on the same spatial domain every year. Finally, the spatiotemporal approach can estimate the coefficient of variation of the standardized CPUE, which is important for data-weighting in stock assessments. It is worth noting that the estimated coefficient of variation was greatest in the first decade of the time series, when the spatial coverage of the dolphin-associated yellowfin fishery in the EPO was most limited. This time-varying coefficient of variation estimated for the standardized CPUE trend is considered more realistic than the constant coefficient of variation assumed for the nominal CPUE trend in the stock assessment model. In the next phase of this project, we plan to investigate how best to incorporate the standardized index of relative abundance in the stock assessment, and the effects of the incorporation on model outputs.

4.3. Importance of modelling spatiotemporal dynamics by length

The length-composition data for yellowfin in the EPO north of the Equator showed a clear pattern of spatial segregation by length. One possible explanation for this is that small and large yellowfin have different preferred habitats within that region. More specifically, the distinct patterns in predicted catch rates by length group may imply that the preferred habitat of yellowfin changes from coastal to pelagic regions over the lifespan of the fish. In addition to these environmental drivers, the spatial segregation pattern could also be caused by spatial patterns in growth rates or fishing effort. Another important

topic for future research is the relationship between size-specific spatiotemporal residuals. In this preliminary study, we specified that the spatiotemporal residuals for both the encounter probability and the positive catch rate were identical and independent among the nine length groups. However, VAST also allows for internally estimating the correlation matrix for size-specific spatiotemporal residuals. If the correlation pattern in the spatiotemporal residuals is also clear, this information could be used to improve the spatial management of the dolphin-associated yellowfin fishery, by predicting preferred fishing grounds (for instance, where only large yellowfin are abundant). In the EPO, both environmental conditions and the predicted catch rates by length showed large spatiotemporal variation. Therefore, being able to accurately predict the location of “hotspots” for catching large yellowfin is extremely valuable for the industry and the conservation of the stock.

ACKNOWLEDGEMENTS

Special thanks to Jim Thorson and Jin Gao for helping with VAST.

REFERENCES

- Francis, R.I.C.C. 2011. Data weighting in statistical fisheries stock assessment models. *Canadian Journal of Fisheries and Aquatic Sciences* 68(6): 1124-1138.
- IATTC, 2017. Tuna, billfishes and other pelagic species in the eastern Pacific Ocean in 2016. IATTC Fisheries Status Report 15.
http://www.iattc.org/PDFFiles/FisheryStatusReports/_English/FisheryStatusReport15.pdf
- Lennert-Cody, C.E., Minte-Vera, C.V., Maunder, M.N., and Aires-da-Silva, A.M. 2013. Indices of relative abundance of yellowfin tuna derived from purse-seine catch and effort data.
http://www.iattc.org/Meetings/Meetings2013/May/_English/SAC-04-04c-YFT-PS-CPUE-indices.pdf
- Maunder, M.N., Thorson, J.T., Lee, H.H., Kai, M., Chang, S.K., Kitakado, T., Albertsen, C.M., Lennert-Cody, C.E., Aires-da-Silva, A.M., and Piner, K.R. 2017. The need for spatial-temporal modeling of catch-per-unit-effort data when used to derived indices of relative abundance to include in stock assessment models. https://www.iattc.org/Meetings/Meetings2017/SAC-08/PDFs/Docs/_English/SAC-08-05d_Spatial-temporal-modeling-of-CPUE-data.pdf
- Minte-Vera, C.V., Aires-da-Silva, A.M., and Maunder, M.N. 2017. Status of yellowfin tuna in the eastern Pacific Ocean in 2016 and outlook for the future.
http://www.iattc.org/Meetings/Meetings2017/SAC-08/PDFs/Docs/_English/SAC-08-04b_Yellowfin-tuna-assessment-for-2016.pdf
- Scott, M.D., Chivers, S.J., Olson, R.J., Fiedler, P.C., and Holland, K. 2012. Pelagic predator associations: tuna and dolphins in the eastern tropical Pacific Ocean. *Marine Ecology Progress Series* 458: 283-302.
- Thorson, J.T., Shelton, A.O., Ward, E.J., and Skaug, H.J. 2015. Geostatistical delta-generalized linear mixed models improve precision for estimated abundance indices for West Coast groundfishes. *ICES Journal of Marine Science* 72(5): 1297-1310.

Figures

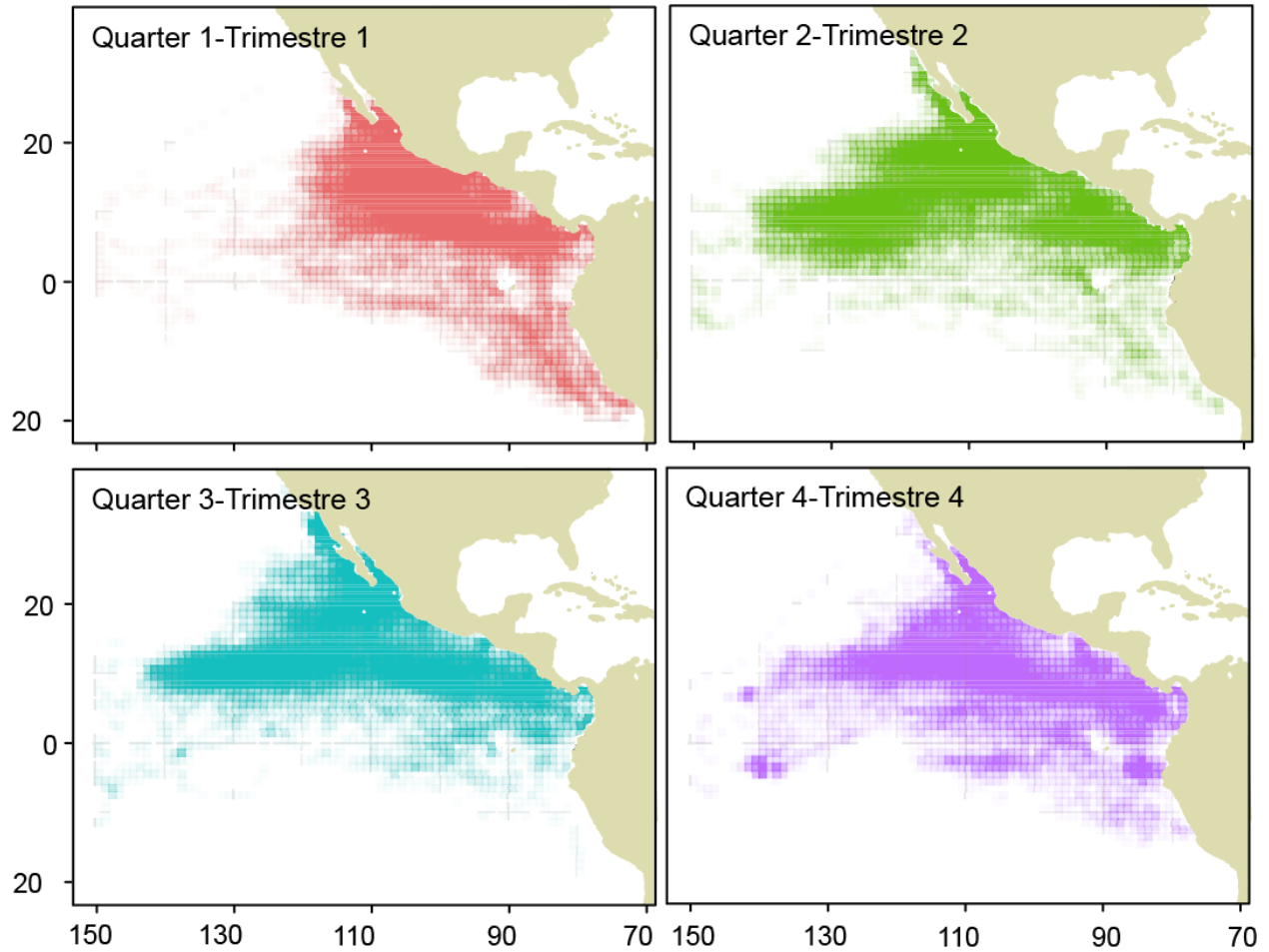


FIGURE 1. Geographic distribution of the CPUE observations of purse-seine vessels that made more than 75% of their sets on tunas associated with dolphins, by quarter, 1975-2016.

FIGURA 1. Distribución geográfica de las observaciones de CPUE de buques cerqueros que realizaron más del 75% de sus lances sobre atunes asociados a delfines, por trimestre, 1975-2016.

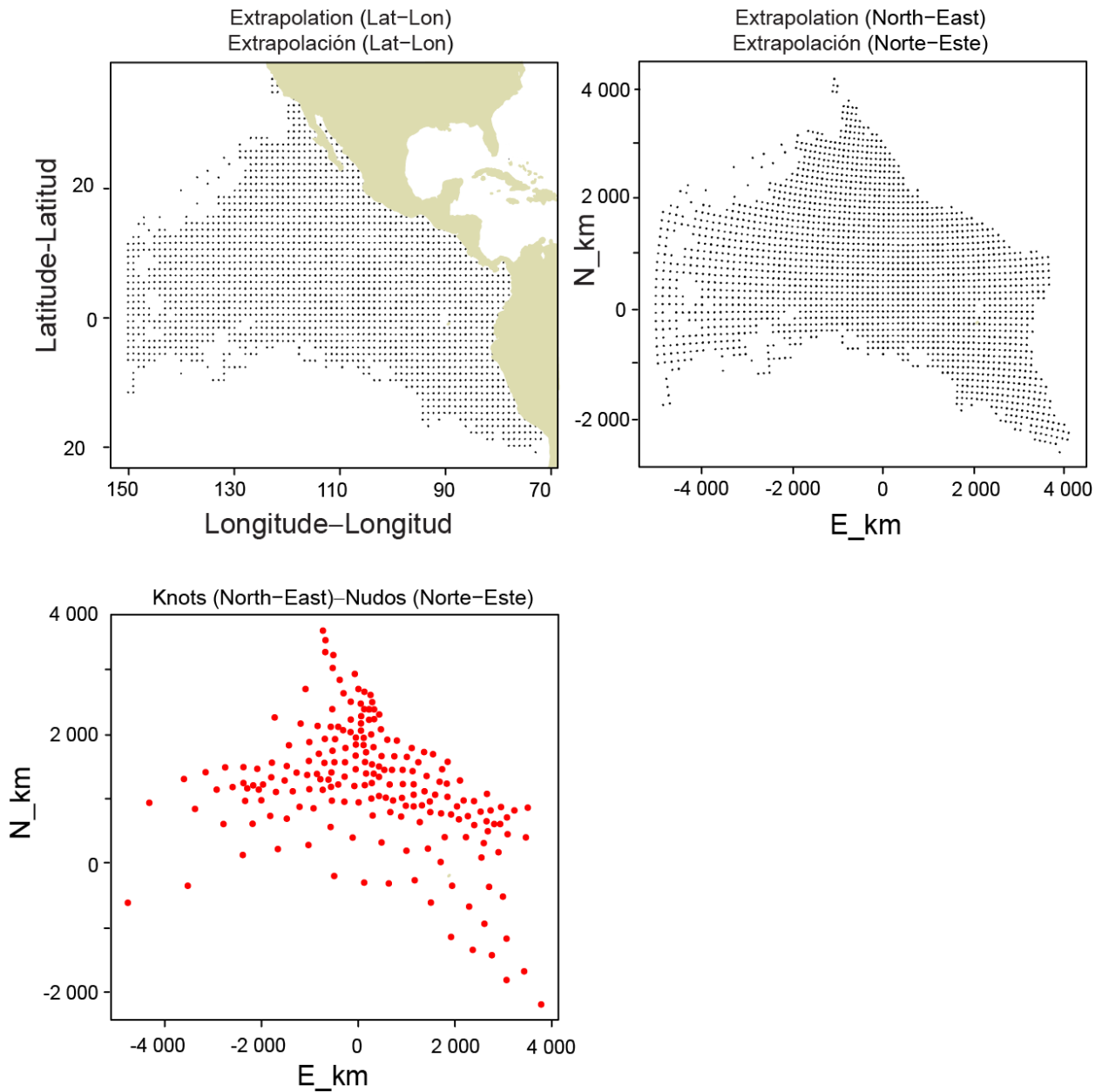


FIGURE 2. Geographic distributions of the per-set CPUE observations used to estimate the index of relative abundance of yellowfin in the EPO (top, in both Lat-Lon and Northing-Easting coordinates), and the corresponding 400 spatial knots generated using the k -means algorithm (bottom, in Northing-Easting coordinates). The spatiotemporal model used the Northing-Easting coordinates to calculate the Cartesian distance between two observations.

FIGURA 2. Distribución geográfica de las observaciones de CPUE por lance usadas para estimar el índice de abundancia relativa de atún aleta amarilla en el OPO (arriba, en Lat-Lon y coordenadas *Northing-Easting*), y los 400 nudos espaciales correspondientes generados usando el algoritmo de k -medias (abajo, en coordenadas *Northing-Easting*). El modelo espaciotemporal usó las coordenadas *Northing-Easting* para calcular la distancia cartesiana entre dos observaciones.

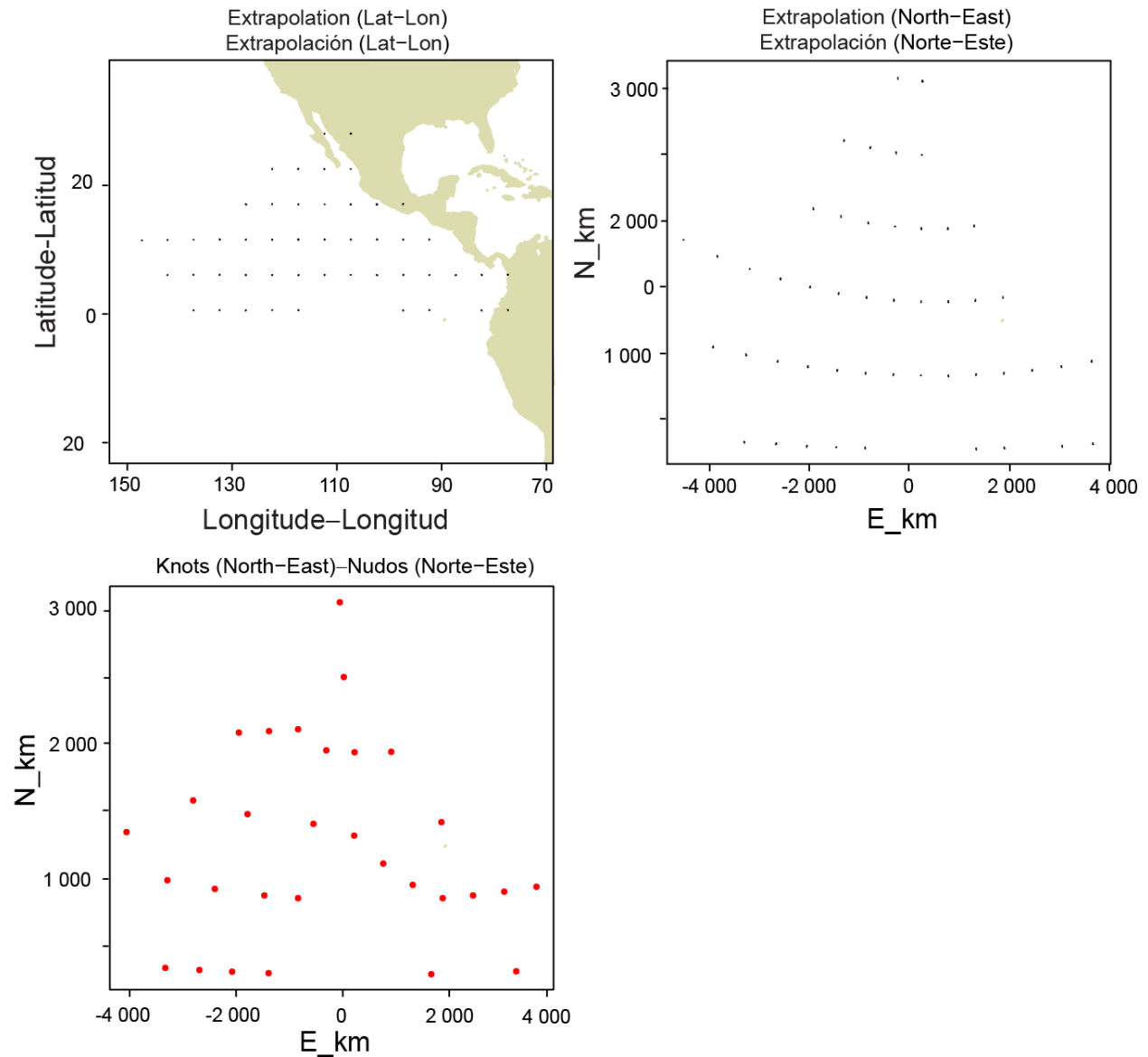


FIGURE 3. Geographic distributions of the yellowfin length-composition observations in the EPO (top, in both Lat-Lon and Northing-Easting coordinates), and the corresponding 30 spatial knots generated using the *k*-means algorithm (bottom, in Northing-Easting coordinates). The spatiotemporal model used the Northing-Easting coordinates to calculate the Cartesian distance between two observations.

FIGURA 3. Distribución geográfica de las observaciones de composición por talla de atún aleta amarilla en el OPO (arriba, en Lat-Lon y coordenadas *Northing-Easting*), y los 30 nudos espaciales correspondientes generados usando el algoritmo de *k*-medias (abajo, en coordenadas *Northing-Easting*). El modelo espaciotemporal usó las coordenadas *Northing-Easting* para calcular la distancia cartesiana entre dos observaciones.

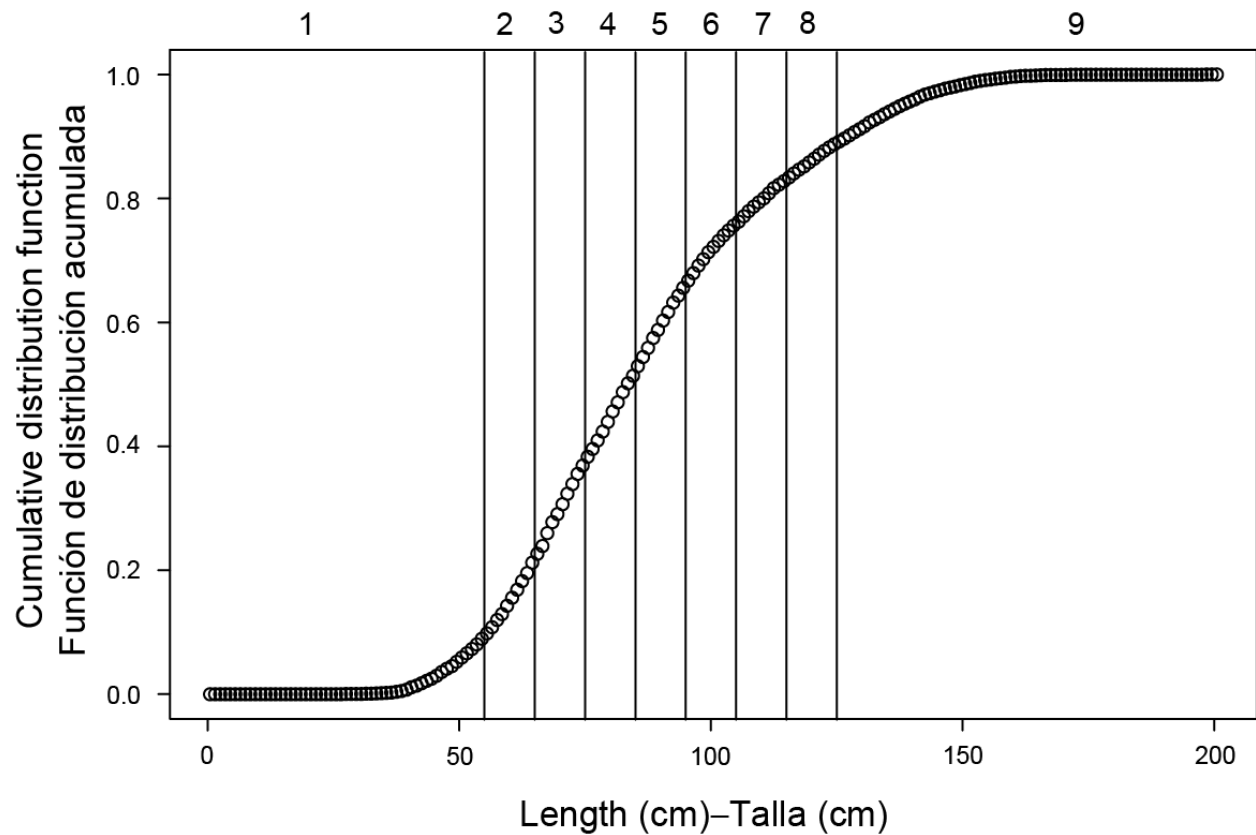


FIGURE 4. Cumulative distribution function of catch-at-length of yellowfin tuna in the dolphin-associated purse-seine fishery in the EPO in quarter 2. The length-composition data were divided into 9 length groups for the spatiotemporal analysis.

FIGURA 4. Función de distribución acumulada de la captura por talla de atún aleta amarilla en la pesquería de cerco asociada a delfines en el OPO en el trimestre 2. Los datos de composición por talla fueron divididos en 9 grupos de talla para el análisis espaciotemporal.

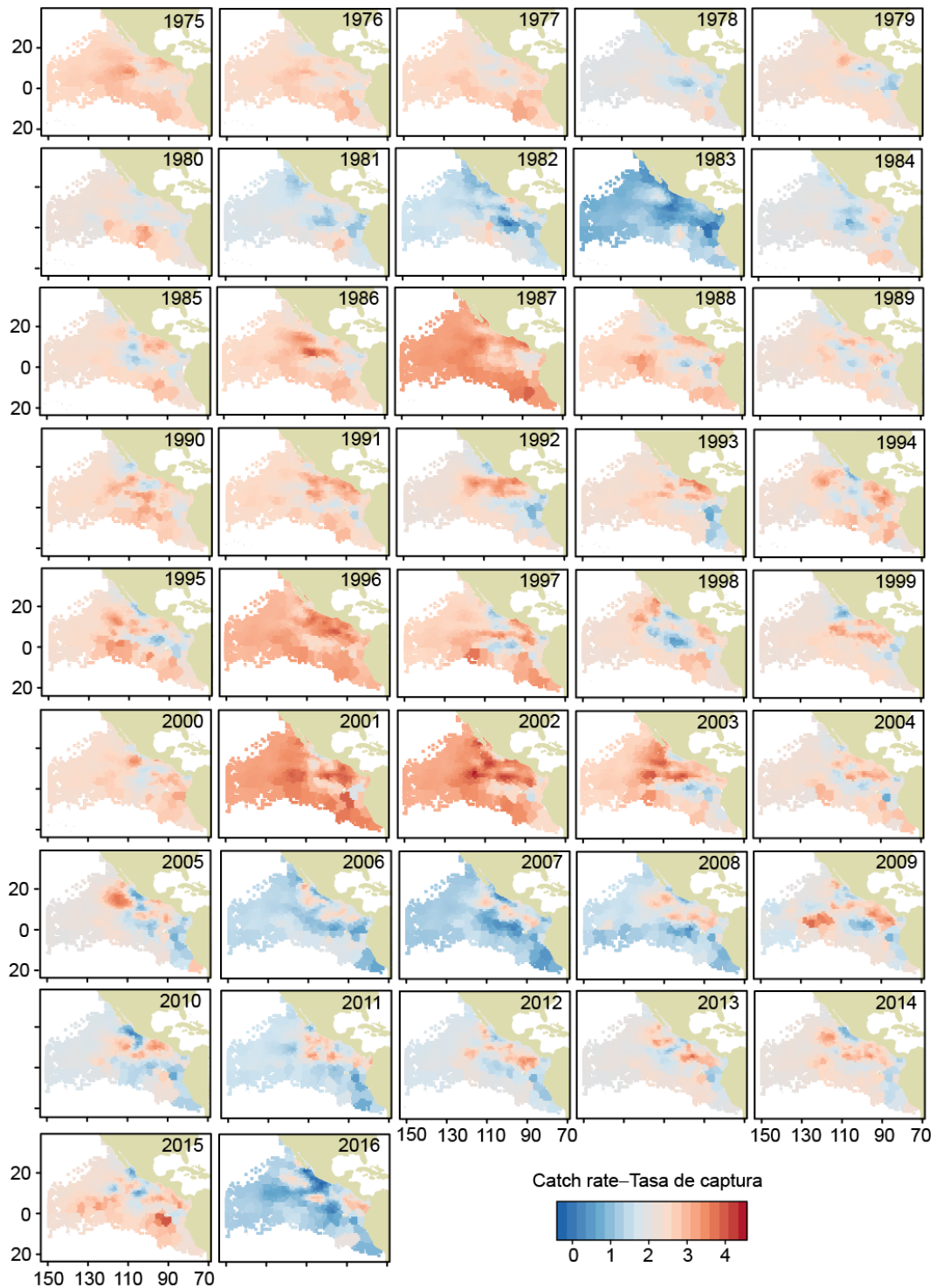


FIGURE 5a. Spatiotemporal distribution of the predicted log catch rate, in tons per day, of yellowfin tuna in the EPO in quarter 1, 1975-2016.

FIGURA 5a. Distribución espaciotemporal del logaritmo de la tasa de captura predicha, en toneladas por día, de atún aleta amarilla en el OPO en el trimestre 1, 1975-2016.

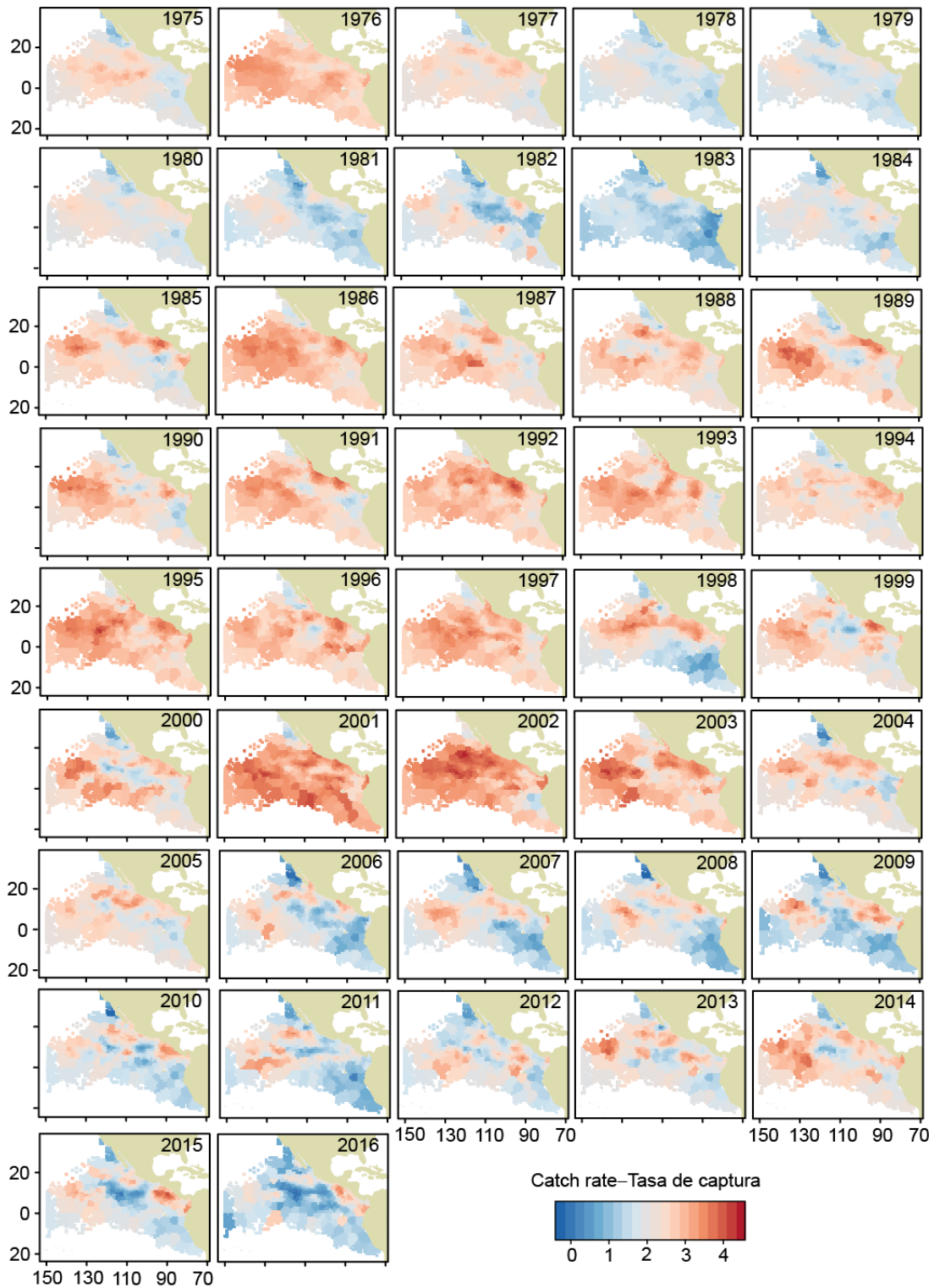


FIGURE 5b. Spatiotemporal distribution of the predicted log catch rate, in tons per day, of yellowfin tuna in the EPO in quarter 2, 1975-2016.

FIGURA 5b. Distribución espaciotemporal del logaritmo de la tasa de captura predicha, en toneladas por día, de atún aleta amarilla en el OPO en el trimestre 2, 1975-2016.

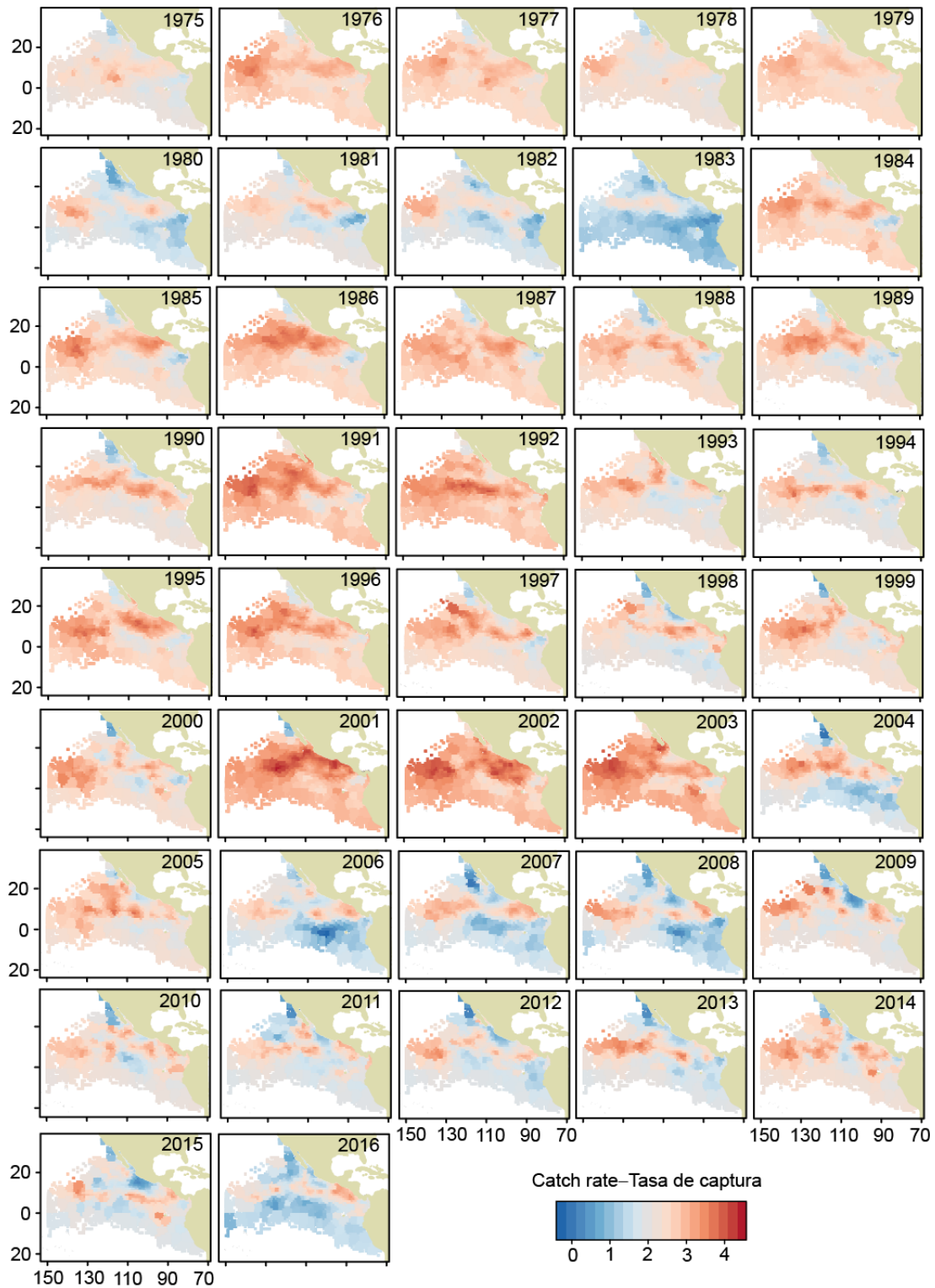


FIGURE 5c. Spatiotemporal distribution of the predicted log catch rate, in tons per day, of yellowfin tuna in the EPO in quarter 3, 1975-2016.

FIGURA 5c. Distribución espaciotemporal del logaritmo de la tasa de captura predicha, en toneladas por día, de atún aleta amarilla en el OPO en el trimestre 3, 1975-2016.

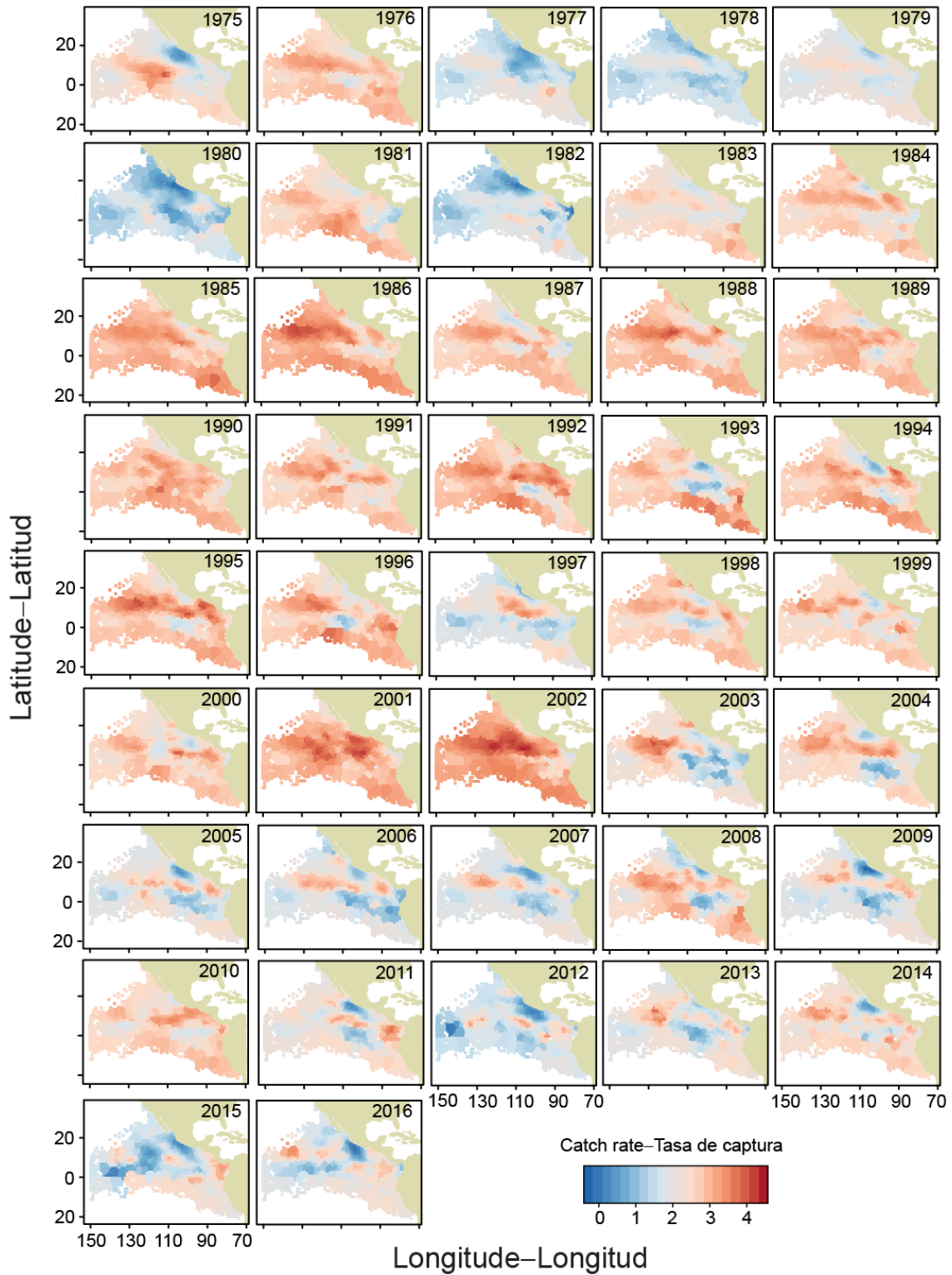


FIGURE 5d. Spatiotemporal distribution of the predicted log catch rate, in tons per day, of yellowfin tuna in the EPO in quarter 4, 1975-2016.

FIGURA 5d. Distribución espaciotemporal del logaritmo de la tasa de captura predicha, en toneladas por día, de atún aleta amarilla en el OPO en el trimestre 4, 1975-2016.

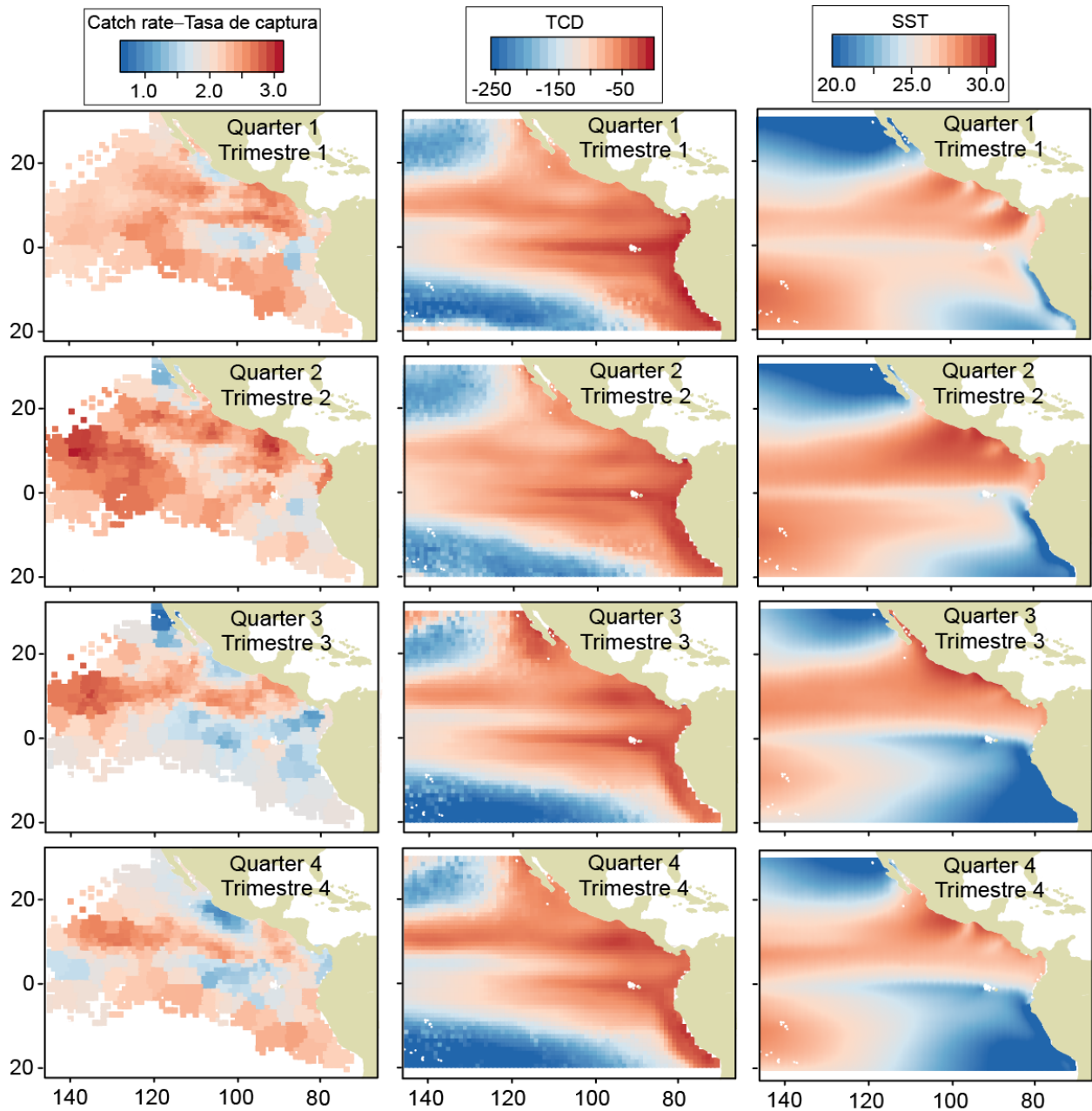


FIGURE 6. Historical mean predicted log catch rate, in tons per day, thermocline depth (TCD), in meters, and sea-surface temperature (SST), in °C, by quarter, 1975-2016.

FIGURA 6. Logaritmo de la tasa de captura media histórica predicha, en toneladas por día, profundidad de la termoclina (PTC), en metros, y temperatura superficial del mar (TSM), en °C, por trimestre, 1975-2016.

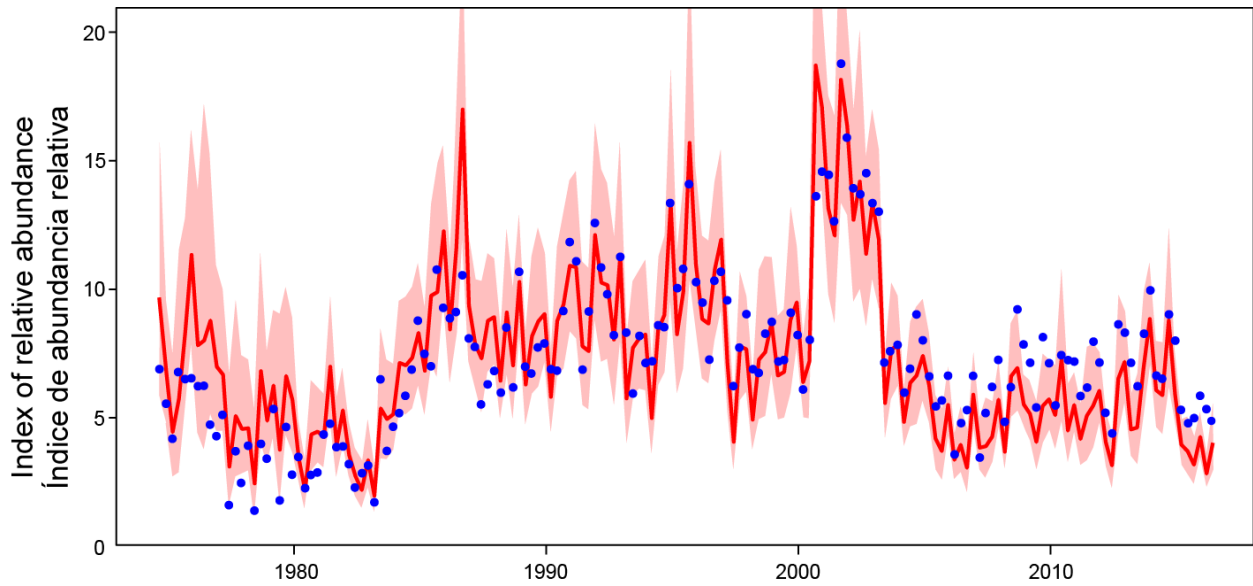


FIGURE 7. Nominal (blue dots) and standardized (red line) indices of relative abundance of yellowfin tuna in the EPO. The shaded area indicates the 95% confidence interval of the standardized index.

FIGURA 7. Índice de abundancia relativa nominal (puntos azules) y estandarizado (línea roja) del atún aleta amarilla en el OPO. El área sombreada indica el intervalo de confianza de 95% del índice estandarizado.

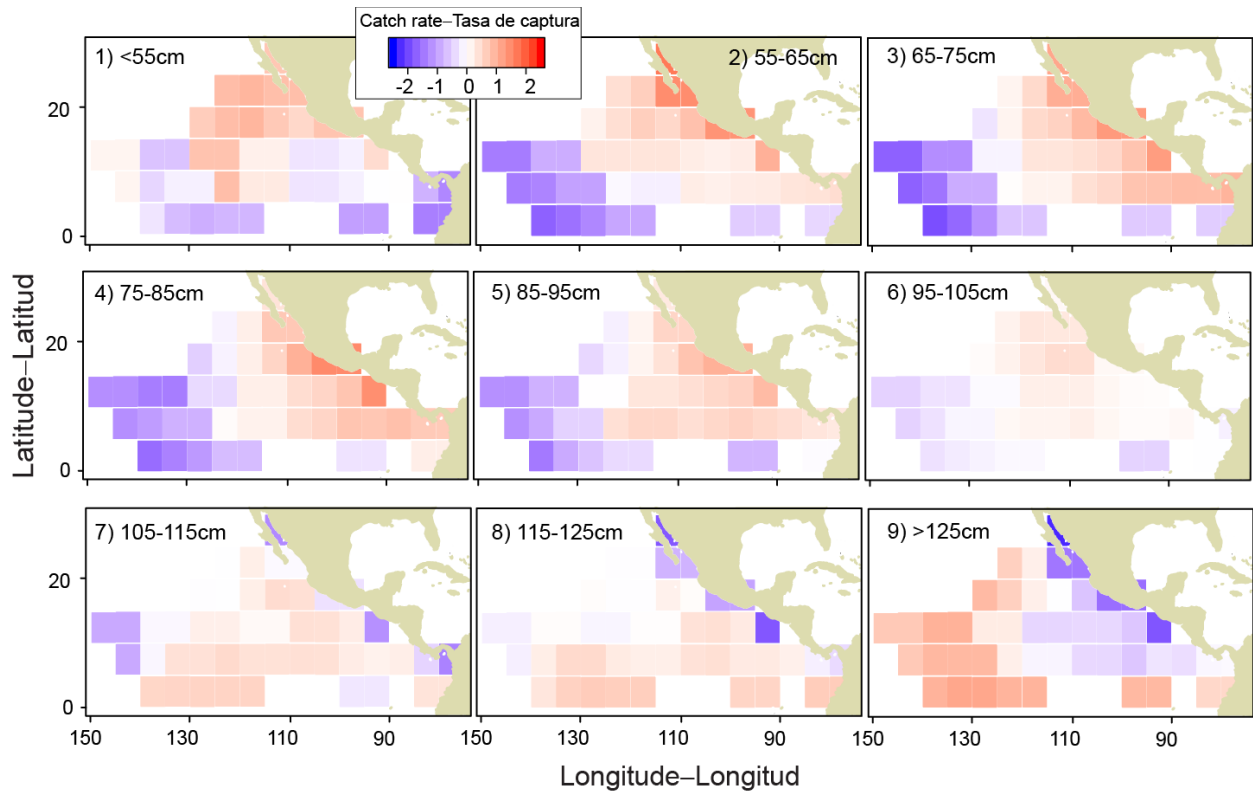


FIGURE 8. Historical mean normalized log catch rate of yellowfin tuna in the EPO for each of the nine length groups considered in the spatiotemporal length-composition analysis.

FIGURA 8. Logaritmo de la tasa de captura media histórica normalizada del atún aleta amarilla en el OPO correspondiente a cada uno de los nueve grupos de talla considerados en el análisis espaciotemporal de composición por talla.